Experimental analysis of RC Dapped Ends Reinforced with Diagonal bars

Analisi Sperimentale di Selle Gerber in C.A. con Armature Diagonali

Maurizio Orlando[1], Giovanni Menichini[2], Heikki Alho[3], Juuso Auvinen[4], Jukka Haavisto[5], Anssi Laaksonen[6]

[1-2] *Department of Civil and Environmental Engineering, University of Florence, Florence, Italy*

[3-6] *Department of Civil Engineering – Research Group of Concrete and Bridge Structures, Tampere University, Tampere, Finland*

[1] Email: maurizio.orlando@unifi.it

[2] Email: giovanni.menichini@unifi.it

[3] Email: heikki.alho@tuni.fi

[4] Email: juuso.auvinen@tuni.fi

[5] Email: jukka.haavisto@tuni.fi

[6] Email: anssi.laaksonen@tuni.fi

ABSTRACT: The strength of reinforced concrete (RC) dapped ends is commonly evaluated using Strut-and-Tie (S&T) models. However, the literature and normative S&T models are limited to configurations with either horizontal and vertical ties or only diagonal ties, both assuming that ties are isolated or concentrated within a narrow zone. An experimental and numerical research has been developed to identify S&T models for dapped ends that include horizontal, vertical, and diagonal ties simultaneously, also considering cases where ties consist of distributed reinforcement bars. Bending tests were performed on full-scale dapped end specimens with three reinforcement layouts: (1) horizontal and vertical ties only, (2) predominantly diagonal ties, and (3) a combination of both. Before casting, the steel bars were instrumented with distributed fibre optic sensors and electrical strain gauges to measure strain. The present paper focuses exclusively on the tests performed on specimens with predominantly diagonal reinforcement of the same amount; results of the other tests will be presented in future works. / La resistenza delle selle Gerber in calcestruzzo armato è comunemente valutata mediante modelli tirante-puntone. Tuttavia, i modelli S&T presenti in letteratura e nelle normative sono limitati a configurazioni con tiranti orizzontali e verticali oppure solo diagonali, assumendo in entrambi i casi che i tiranti siano isolati o concentrati in una zona ristretta. È stata condotta una ricerca sperimentale e numerica di selle Gerber nelle quali siano presenti contemporaneamente armature orizzontali, verticali e diagonali, considerando anche i casi in cui le armature siano distribuite. Sono state eseguite prove a flessione su selle Gerber con tre differenti configurazioni di armatura: (1) solo armature orizzontali e verticali, (2) armature prevalentemente diagonali e (3) una combinazione delle due precedenti disposizioni. Prima del getto, le barre di acciaio sono state strumentate con sensori estensimetrici ottici ed elettrici per la misura delle deformazioni. Il presente articolo si concentra esclusivamente sulle prove eseguite su provini con armatura prevalentemente diagonale; i risultati delle altre prove saranno presentati in lavori successivi.

KEYWORDS: dapped-end beams; experimental tests; nonlinear FEM; S&T models; ultimate capacity / selle Gerber; prove sperimentali; modelli non lineari agli elementi finiti; modelli tirante-puntone; capacità resistente ultima.

1 INTRODUCTION

The paper deals with dapped-end beams, reinforced concrete elements widely used in existing bridges in Europe, particularly between the 1950s and 1970s (di Prisco et al. 2023, Santarsiero et al. 2023). They were adopted to simplify construction, allow statically determinate structural schemes, reduce the effects of differential settlements and thermal actions, and limit overall structural depth. Dapped ends represent geometric discontinuity regions, where classical Navier-Bernoulli beam theory does not hold, due to the presence of high stress concentrations. The load-transfer mechanism can be approximated with truss models, with concrete struts and steel ties (Mattock & Chan 1979; Schlaich et al. 1987). Their behavior is governed by the complex interaction of shear, bending, anchorage, and local compressive stresses, which may result in brittle failure if not properly detailed. Strut-and-Tie (S&T) models represent the common design and assessment tool for these regions. Building codes such as Eurocode 2 typically offer two alternative S&T models, both designed for concentrated steel bars. One can be used for dapped ends equipped with horizontal and vertical ties (hanger reinforcement) and one for dapped ends with diagonal ties. Experimental research has consistently demonstrated that the reinforcement arrangement plays a decisive role in the behavior of dapped-end beams. Early laboratory investigations clarified the fundamental load-transfer mechanisms and typical failure modes, while more recent full-scale tests have em-

phasized the importance of detailing and bar configuration in governing strength and ductility (Desnerck et al. 2016; Flores Ferreira et al. 2023; Menichini et al. 2025). However, many existing structures feature reinforcement layouts that do not strictly follow the configurations assumed in current S&T models. Reinforcement is frequently more dispersed or includes a combination of horizontal, vertical, and diagonal bars, reflecting design practices developed before S&T methods became standard. In these situations, applying the Eurocode 2 S&T models directly can be challenging, and the interaction of multiple load-transfer mechanisms is often presumed rather than experimentally verified. Although analytical and numerical models are widely used to interpret experimental findings (Flores Ferreira et al. 2025), physical testing remains crucial to capture the real structural response of dapped ends, particularly when different reinforcement schemes and overlapping S&T mechanisms are present. Experimental studies provide essential insight into cracking evolution, failure modes, stress redistribution, and deformation capacity, forming a reliable basis for the assessment of existing structures and the refinement of design approaches. Consequently, experimental investigation continues to be fundamental for both bridge and precast concrete structures facing increasingly demanding safety and performance requirements.

1.1 *Aim of the work*

This study reports results of experimental tests on two RC dapped ends with predominantly diagonal bars.

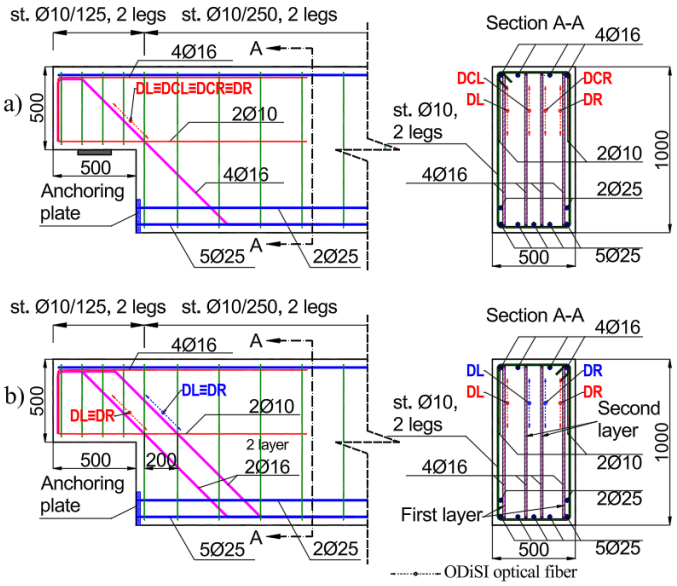

Figure 1. Reinforcement layout of specimens B2C (a) and B2D (b) / Disposizione delle armature dei provini B2C (a) e B2D (b).

The first specimen includes one layer of four Φ16 diagonal bars, while the second is equipped with two layers, each consisting of two Φ16 diagonal bars. The two specimens are part of a more extended experimental campaign, which includes a total of eight specimens with different reinforcement layouts. Results of the remaining six specimens will be presented in future work. Bending tests to failure were conducted at Tampere University. The structural response of specimens was also assessed numerically through nonlinear FE models and compared with experimental results. Finally, the experimental results were also compared with predictions from strut-and-tie models.

The aim of this study is to compare the cracking behaviour, steel stress distribution, and ultimate load-carrying capacity of two dapped-end specimens containing the same amount of diagonal reinforcement arranged in two different layouts.

2 EXPERIMENTAL PROGRAM

2.1 *Specimens and reinforcement layout*

The experimental campaign includes full-scale reinforced concrete beams with identical global geometry, designed to study dapped-end behavior (Fig. 1). Each beam has a total length of 6800 mm, a height of 1000 mm, and a width of 500 mm. The longitudinal reinforcement consists of seven Ø25 bars. Steel plates were welded to the longitudinal bar ends to prevent slippage because bent-up bars would have influenced the D-region.

The dapped-end region is reinforced with a combination of longitudinal bars, vertical stirrups (Ø10), horizontal U-bars (Ø10), and diagonal bars (Ø16), arranged to ensure shear transfer and force redistribution within the disturbed region. The present study focuses on two specimens, denoted as B2C and B2D, which share identical geometry, material properties, and overall reinforcement detailing. The only difference between the two configurations lies in the arrangement of the diagonal reinforcement. In specimen B2C, four Ø16 diagonal bars are arranged in a single concentrated layer, forming a well-defined tensile tie within the dapped-end region. In specimen B2D, the same amount of diagonal reinforcement is distributed over two layers (2+2 configuration). This configuration allows investigating the influence of the spatial distribution of diagonal reinforcement on the load-transfer mechanism, while keeping all other parameters unchanged.

2.2 *Test set up and instrumentation*

The experimental tests were carried out using a four-point bending configuration. The load was applied through hydraulic actuators connected to a system of rods and a spreader beam, ensuring uniform load distribution. The dapped end was supported on roller support, while the main span was supported by a pinned condition. Steel plates and intermediate pads were used at loading and support locations to avoid concentration of local stress (Fig. 2).

A comprehensive instrumentation system was implemented to monitor both global and local structural response. In addition to load cells and displacement transducers, optical fibre sensors (ODiSI) and electrical strain gauges were used. The optical fibre sensors had a 240 µm thick acrylate coating and they were glued with cyanoacrylate into a 1.5 mm wide groove in the rebar. The strain gauges were glued with cyanoacrylate to the smoothed surface of the rebar.

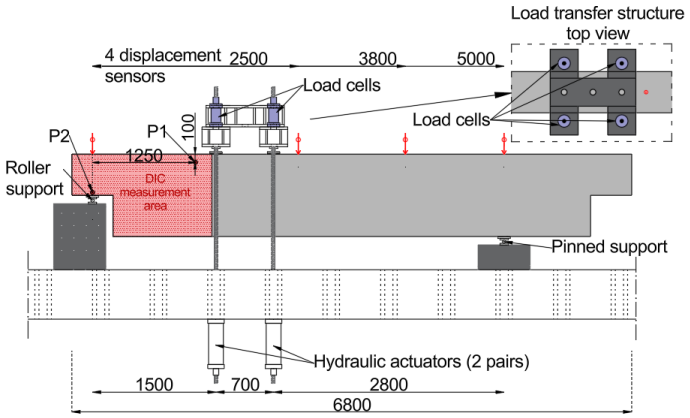

Figure 2. Experimental setup (measurements in mm) / Setup sperimentale (quote in mm).

Optical sensors were installed within selected reinforcement bars, including diagonal bars, horizontal U-bars, bottom longitudinal reinforcement, and first and third stirrup. These sensors provide distributed strain measurements along the bar length, allowing the identification of strain localization, progressive activation of reinforcement, and interaction between different structural components. This level of detail enables a direct comparison with numerical predictions and provides a deeper understanding of the internal load-transfer mechanisms. Strain gauges were installed on different rebars than the optical fibres and were used to expand the number of measured rebars. Both sides of the dapped ends were painted with white and speckled with black dots. One pair of cameras were placed on each side, and the pictures were used for digital image correlation to measure displacements and surface strains.

3 NUMERICAL MODELS

3.1 *Finite element model*

Nonlinear finite element analyses were carried out using two-dimensional models developed in DIANA FEA (2025). The adoption of 2D models in place of more accurate 3D models was motivated by the almost uniform distribution of the reinforcement layers across the transverse section in both specimens B2C and B2D, suggesting that three-dimensional effects would be limited. Concrete was discretized with 8-node plane stress elements (CQ16M), adopting a refined mesh (≈25 × 25 mm) in the dapped-end region up to 1500 mm from the nib, and a coarser mesh (≈50 × 50 mm) in the remaining portions of the beam (Fig. 3). Boundary conditions reproduced the experimental setup, with a roller support at the dapped end and a pinned support along the main span. The load was applied in displacement control through a spreader beam. Pads at supports and loading plates were modelled as linear elastic materials and connected to the concrete through compression-only interfaces. Reinforcement was represented by embedded truss elements, with steel–concrete interaction described by nonlinear bond-slip relationships. The anchorage of the bottom longitudinal bars was simulated using elastic anchor elements. The nonlinear response was solved through an incremental-iterative modified Newton–Raphson procedure, with convergence checked using combined force and energy criteria.

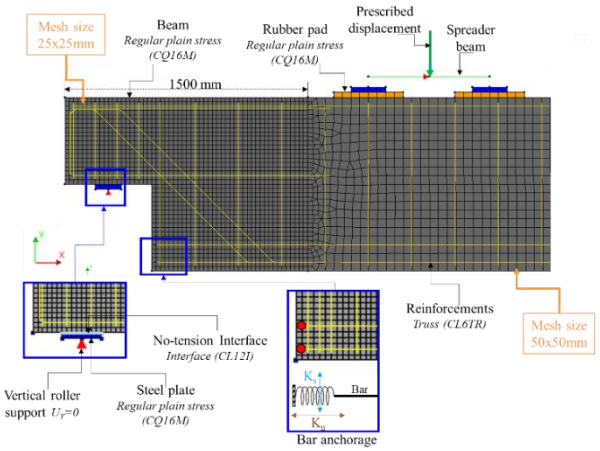

Figure 3. FE numerical model / Modello numerico agli elementi finiti.

3.2 *Material constitutive model*

Concrete was modelled using a total strain-based crack approach, accounting for tensile cracking, compressive crushing, and stiffness degradation (Fig 4).

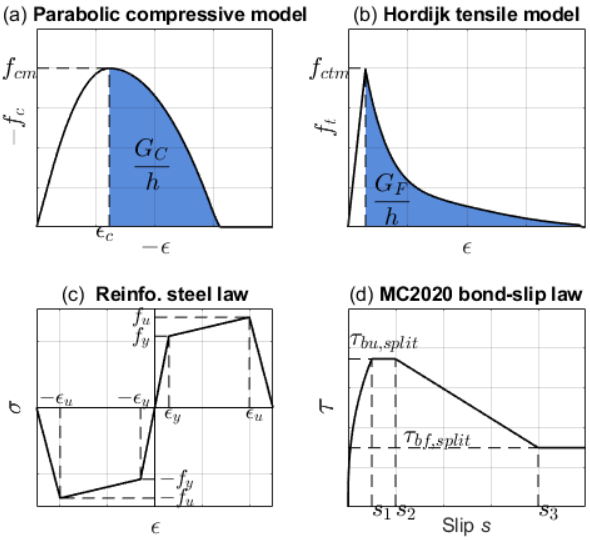

Figure 4. Material constitutive laws: a) Concrete compressive, b) Concrete tensile, c) Reinforcement steel, d) Bond-slip / Leggi costitutive dei materiali: a) Calcestruzzo a compressione, b) Calcestruzzo a trazione, c) Acciaio per armature, d) Aderenza barre-cls.

The compressive response was described by a parabolic stress–strain law, while tensile behaviour followed the softening relationship proposed by Hordijk (1991). The post-peak behaviour in both tension and compression was defined in terms of fracture energy, namely tensile (G_F) and compressive (G_C) fracture energies calculated according to the Nederland Guidelines formulation (Hendriks et al. 2022).
Crack development was simulated using a rotating crack model, suitable for monotonic loading conditions. The interaction between steel and concrete was explicitly considered through nonlinear bond–slip relationships calibrated according to fib Model Code 2020 (fib 2023). The maximum bond stress was defined as a function of bar diameter and position, ranging from approximately 9.6 MPa for the Ø25 longitudinal bars to about 15.6 MPa for the Ø10 U-bars. Reinforcement was modelled using embedded truss elements governed by a bilinear elastic-plastic constitutive law with isotropic strain hardening. The mechanical properties of materials, experimentally derived, adopted in the analyses are summarized in Table 1 and 2.

Table 1. Mechanical parameters and constitutive laws for concrete in the numerical model / Parametri meccanici e leggi costitutive del calcestruzzo nel modello numerico.

Concrete			
Modulus of elasticity	E	32837	N/mm^2
Poisson's ratio	ν	0.2	
Compressive behaviour		*Parabolic*	
Compressive strength	f_{cm}	38	N/mm^2
Compressive fracture energy	G_C	27.73	N/mm
Strain at the maximum stress	ε_{c1}	19.3‰	
Ultimate strain	ε_{cu}	45.7‰	
Tensile behaviour		*Hordijk*	
Average tensile strength,	f_{ctm}	2.90	N/mm^2
Tensile fracture energy	G_F	0.098	N/mm^2

Table 2. Mechanical parameters of steel bars / Parametri meccanici delle barre di armatura.

Reinforcement steel				
Diameter [mm]	ε_y [%]	f_y [N/mm^2]	ε_u [%]	f_u [N/mm^2]
10	0.263	527	21.5	676
12	0.270	540	20.5	683
16	0.278	556	23.5	677
25	0.268	535	22.3	658

4 ANALYTICAL MODELS

4.1 *Strut-and-Tie models*

The load-carrying capacity of the dapped ends was assessed using Strut-and-Tie (S&T) models, adopting simplified representations of the internal force transfer mechanisms within the disturbed region. A nominal concrete compressive strength of 35 MPa was assumed, while the steel yield and ultimate tensile strengths were taken as 535 MPa and 630 MPa, respectively. For the diagonal reinforcement, the reference strut-and-tie scheme proposed by Eurocode 2 is adopted (Fig. 5b). In specimen B2D, which featured two layers of diagonal bars, tie T1 is positioned at the centroid of the reinforcement, following common design practice. For both specimens, the number of stirrups contributing to the strut-and-tie (S&T) load-resisting mechanism is determined through an iterative procedure (Menichini et al., 2024). Initially, only the first stirrup is considered; subsequently, at each iteration, the contribution of an additional stirrup is added until either yielding/rupture of the horizontal reinforcement in the nib, or crushing of the concrete, occurs.
The load capacity was evaluated considering both the steel yield strength and the ultimate tensile strength, to assess the influence of the assumed stress level in the reinforcement. The resulting predictions are compared with experimental and numerical results in the following sections.

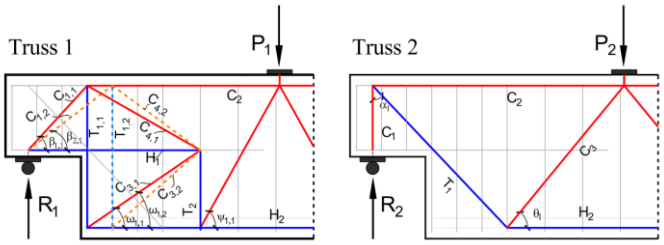

Figure 5. S&T models a) iterative approach according to Menichini et al. (2024), b) EC2 model involving diagonal bar / Modelli S&T: a) approccio iterativo secondo Menichini et al. (2024), b) modello EC2 con barra diagonale.

4.2 *Sectional approach*

Beside the S&T models, the load capacity can be also assessed using sectional approach (Del Giudice 1967; Menichini et al. 2024): the increase in the ultimate reaction at the support is taken as the minimum of the ultimate shear strength (V) at section S (Figure 6) and the vertical component of the ultimate eccentric tensile axial force (N) at section S_1, inclined at 45°.

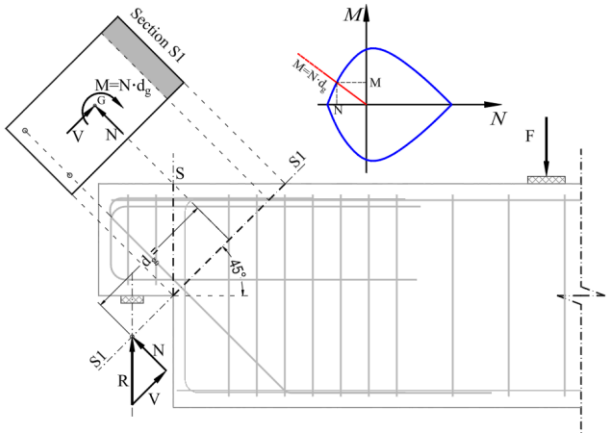

Figure 6. Sectional model / Modello sezionale.

In turn the ultimate axial force N is determined by the intersection between the moment-axial force interaction curve of section S_1 and the line describing the relationship between bending moment and axial force, $M=N \cdot d_g$, where the slope of the line is equal to the eccentricity d_g (Fig. 6). Besides diagonal bars the contributions of U-bars and the first vertical bars are considered by projecting their axial forces normal to section S_1.

5 RESULTS

5.1 *Global response and load-carrying capacity*

The global structural response of specimens B2C and B2D is evaluated in terms of load–displacement behaviour and ultimate load capacity. The experimental results are compared with predictions obtained from finite element analyses, Strut-and-Tie (S&T) models, and sectional approaches (Fig 7). The load–displacement curves show a similar initial stiffness for both specimens, followed by a nonlinear response governed by cracking and progressive stress redistribution within the dapped-end region. Specimen B2C reaches a higher ultimate load compared to B2D, confirming the influence of the diagonal reinforcement layout on the structural capacity.

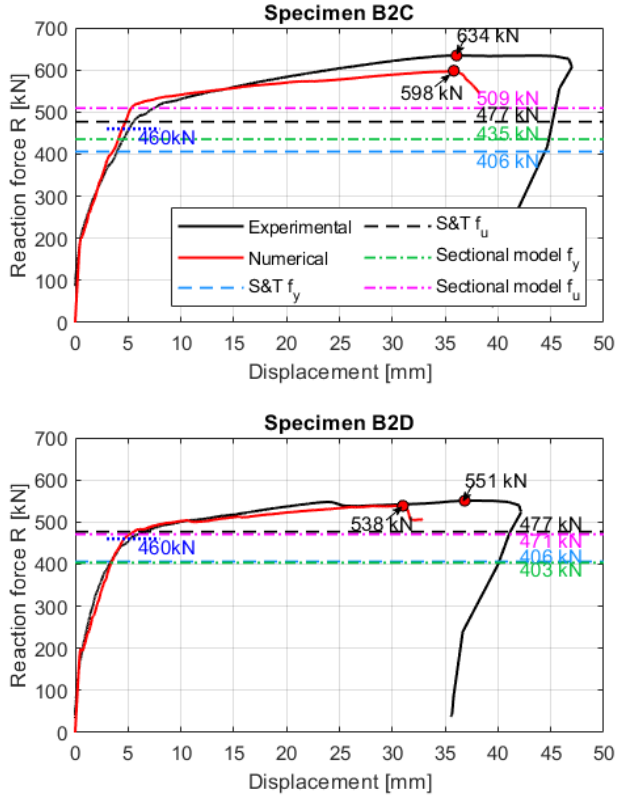

Figure 7. Comparison between experimental and numerical load-displacement curves and analytical load limits / Confronto tra le curve carico-spostamento sperimentali e numeriche e i limiti di carico analitici.

The finite element models provide accurate predictions of the peak load, with differences of approximately 5.7% for B2C and 2.3% for B2D relative to the experimental results (Table 3). In addition, the numerical simulations are able to reproduce the overall shape of the response, including stiffness degradation and the nonlinear evolution up to failure.

As expected, both Strut-and-Tie and sectional approaches provide conservative estimates of the load-carrying capacity confirming the limitations of simplified analytical methods when applied to disturbed regions. Overall, the results highlight the strong influence of reinforcement layout on structural performance and confirm the ability of nonlinear numerical models to capture the global response with satisfactory accuracy.

Table 3. Maximum support reaction R at the nib: numerical, S&T and sectional model results vs experimental data / Reazione massima R all' appoggio sotto la sella: risultati dei modelli numerici, S&T e sezionali rispetto ai dati sperimentali.

Specimen	Experimental [kN]	S&T model [kN]		Sectional model [kN]		Numerical model [kN]
		f_y	f_u	f_y	f_u	
B2C	634	406	477	399	473	598
		-36.0%	*-24.8%*	*-37.0%*	*-25.5%*	*-5.7%*
B2D	551	406	477	403	471	538
		-26.3%	*-13.4%*	*-26.8%*	*-14.5%*	*-2.3%*

5.2 *Crack pattern*

The crack development in specimens B2C and B2D was analysed by comparing experimental observations and numerical results at the same reference load of 460 kN, corresponding to the point indicated in the load–displacement curves (Fig. 7). This load represents different stages of the structural response, approximately 72.5% of the ultimate load for B2C and 83.5% for B2D. The relationship between crack patterns and reinforcement stress levels is illustrated in Figure 8. Stresses were obtained by converting the recorded strains using the experimental stress–strain laws of the reinforcement bars. Experimental crack patterns were processed and reconstructed using digital image correlation and the Automated Crack Detection and Measurement (ACDM) (Gehri et al. 2020 and 2022).

Both specimens exhibit widespread cracking in the dapped-end region, driven by the interaction of compressive and tensile forces. However, the spatial arrangement of the diagonal reinforcement affects crack morphology. In B2D (Fig. 8b), with two layers of diagonal bars, the main crack is wider at the re-entrant corner than in B2C (Fig. 8a), indicating more deformation at this area. As a result, higher tensile stresses in the reinforcing bars leads to developing of several smaller cracks beneath the main crack. Yielding of both diagonal and longitudinal reinforcement are spread over a wider region.

Specimen B2C exhibits high stress concentrations localized at the intersections between the diagonal bars

and the main corner cracks. This configuration provides an effective clamping action on the cracks, contributing to the control of crack width. However, cracks are propagating higher towards the top edge of the beam than in B2D. Numerical simulations reproduce the main crack trajectories and the damaged zones observed experimentally. The FE model indicates a more distributed cracking pattern for B2C, extending over a larger portion of the dapped-end region. For B2D, the model captures the smaller but wider cracking zone concentrated near the corner, consistent with the experimental observations (Fig. 9).

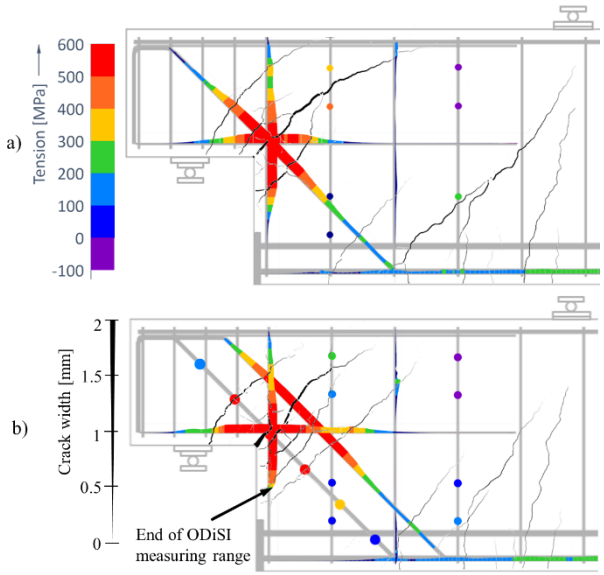

Figure 8. Experimental crack pattern and rebar stress: specimen B2C (a) and specimen B2D (b) / Quadro fessurativo numeric e tensioni nelle barre: provino B2C (a) e provino B2D (b).

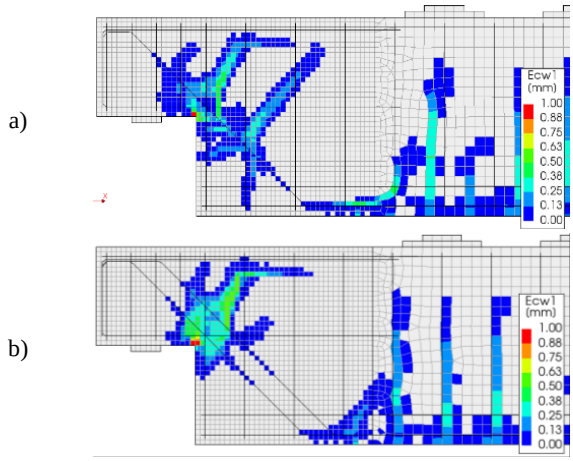

Figure 9. Numerical crack pattern: specimen B2C (a) and specimen B2D (b) / Quadro fessurativo numerico: provino B2C (a) e provino B2D (b).

5.3 *Rebar strains*

The analysis of rebar strains can help understand the internal load-transfer mechanisms. Figures 10 to 12 compare experimental and numerical strains at the reference load of 460 kN. In the plots, the discrete points connected by dashed lines represent electrical strain gauge measurements, while the continuous lines represent the distributed strain data obtained via ODiSI optical fibres. The numerical results are indicated by the blue lines, and the red dashed line marks the yielding threshold.

For specimen B2C, with 4Φ16 diagonal bars arranged in a single layer, the sensors are labelled as DL (Left), DCL (Center-Left), DCR (Center-Right), and DR (Right). The diagonal bars in B2C remain generally below the yielding limit, except for localized experimental peaks in the DR coinciding with the intersection of major cracks (Fig 10a).

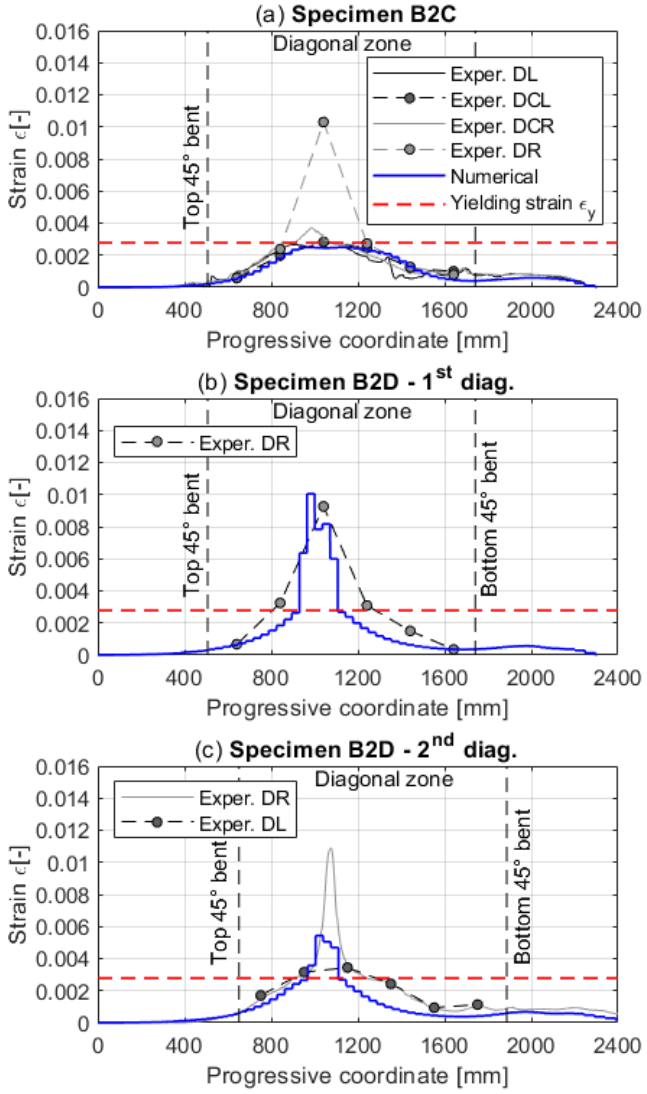

Figure 10. Experimental vs numerical strain in diagonal bars: specimen B2C (a), specimen B2D 1st layer (b) and 2nd layer (c) / Deformazione sperimentale e numerica nelle barre diagonali: provino B2C (a), provino B2D 1° strato (b) e 2° strato (c).

Specimen B2D has two layers of diagonal reinforcement (2+2 Φ16). In Figure 10b and c, DL and DR refer to the left and right bars within each layer. Unlike B2C, the diagonal bars in both layers of B2D reach the yielding strain. Despite this higher activation, B2D reaches a lower ultimate load than B2C. This suggests that distributing the diagonal reinforcement into multiple layers, while increasing local strain levels, may reduce the overall efficiency of the S&T mechanism due to reduction of the internal lever arm of the inclined resisting cross-section S_1 (Fig. 6). The numerical model also accurately captures the location

of the maximum tensile demand, which occurs between 400 mm and 600 mm from the nib interface. At this load level, the strains are mostly within the elastic range and remain below the yielding threshold. It is important to note that the 2D finite element model cannot explicitly capture eventual differences between the two diagonal bars of the same layer, consequently, the numerical prediction represents an averaged value.

The horizontal U-bars (Ø10) play a key role in the dapped-end region as primary ties in Truss 1 (Fig. 5). Figure 11 shows the strain distribution along these bars for both specimens, comparing experimental (ODiSI fibres) and numerical results.

In specimen B2C, the strains show a yielding region, with a peak at the inner corner of the nib where values exceed the yielding threshold. This confirms that the horizontal reinforcement is fully activated at the reference load of 460 kN. The numerical model correctly identifies the location of maximum strain, although it slightly underestimates the peak and predicts a more distributed strain profile.

In specimen B2D, the U-bars show higher strain levels than in B2C, with a sharper and more localized peak at the dapped-end interface. The numerical model again captures the trend and the critical region of activation. The higher strains are consistent with the greater damage observed in B2D at the same load level. In both specimens, the horizontal U-bars reach yielding, confirming their activation. However, the higher strain levels in B2D means the higher activation in this case consistent with wider main crack compared to B2C.

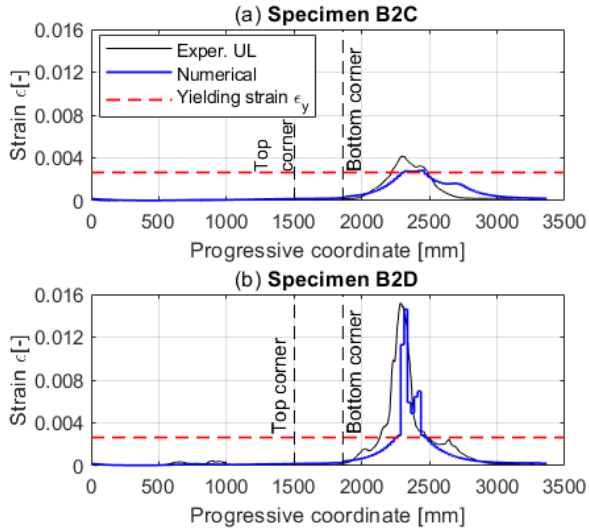

Figure 11. Experimental vs numerical strain in U horizontal bar: a) specimen B2C, b) specimen B2D / Deformazione sperimentale e numerica nella barra orizzontale ad U: a) provino B2C, b) provino B2D.

The activation of the vertical stirrups (Ø10) is strictly dependent on their proximity to the re-entrant corner of the dapped end. Comparison between B2C and B2D highlights differences in transverse reinforcement response. In both specimens, the first stirrup (Fig. 12) is the most heavily loaded: in B2C it barely reaches yielding, while in B2D the strain is higher, addressing a more pronounced activation than in B2C. The activation of the second stirrup is similar in specimens B2C and B2D. In both cases, the third stirrup exhibits only limited activation, as indicated by the very low strain levels recorded. The bottom longitudinal bars remain elastic, with maximum strains of 0.00141 in B2C and, lower, 0.00132 in B2D, well below the yielding threshold of 0.00267.

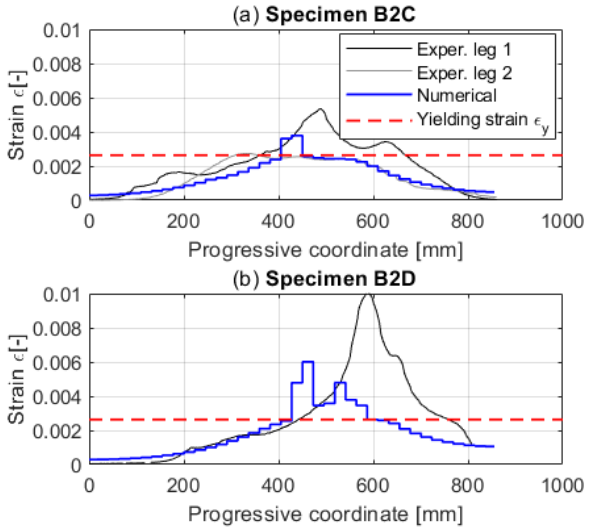

Figure 12. Experimental vs numerical strain in the 1st stirrup: specimen B2C (a), specimen B2D (b) / Deformazione sperimentale e numerica nella prima staffa: provino B2C (a), provino B2D (b).

6 CONCLUSIONS

A numerical and experimental study was conducted on two RC dapped-end beams to investigate load-resisting mechanisms associated with different reinforcement layouts, including horizontal and vertical ties, predominantly diagonal ties, and their combination, in both concentrated and distributed arrangements. This paper focuses on the specimens with predominantly diagonal bars at both ends, while the others will be addressed in future work. The structural response was preliminarily predicted using nonlinear FE models using constitutive laws of materials, fracture energy formulation of concrete, and bond-slip relationship between steel and concrete chosen from previous studies by the same authors. The experimental campaign employed detailed instrumentation, including LVDTs, optical and electrical strain gauges, and DIC, enabling a comprehensive characterization of strain fields and supporting the identification of load-resisting mechanisms. Numerical and experimental results showed good agreement in terms of load-displacement response, ultimate load, crack patterns, and strain distributions.

Both sectional and strut-and-tie (S&T) models underestimate the ultimate capacity, with the latter providing a closer approximation. However, neither approach captures the differences between the two configurations observed in the experimental cam-

paign: the two-layer reinforcement configuration exhibits a lower ultimate capacity, despite having the same total amount of diagonal reinforcement as the single-layer layout. The cracking pattern also differs between the two configurations; however, this comparison should be interpreted with caution, as it is based on a single load level, corresponding to different stages of the structural response.

This suggests that both analytical models have limited sensitivity to how reinforcement distribution affects internal load-transfer mechanisms, highlighting the need for further investigation. / È stato condotto uno studio numerico e sperimentale su selle Gerber in c.a. per studiare i meccanismi resistenti associati a diverse configurazioni di armatura, tra cui armature orizzontali e verticali, armature prevalentemente diagonali e combinazione di armature orizzontali e verticali con armature diagonali, considerando sia barre concentrate che distribuite. Il presente lavoro si concentra su due selle dotate entrambe di armature prevalentemente diagonali, mentre i risultati relativi alle altre selle saranno presentati in studi futuri. Preliminarmente la risposta strutturale è stata valutata mediante modelli agli elementi finiti non lineari utilizzando leggi costitutive dei materiali, formulazioni dell'energia di frattura del calcestruzzo e leggi di aderenza acciaio-calcestruzzo già impiegate con buoni risultati in precedenti studi degli stessi autori. Le misure sperimentali sono state effettuate mediante una strumentazione dettagliata, comprendente trasduttori lineari di spostamento, estensimetri ottici ed elettrici e tecniche di correlazione digitale delle immagini (DIC), che hanno consentito una caratterizzazione completa dei campi deformativi e l'identificazione dei meccanismi resistenti. I risultati numerici e sperimentali hanno mostrato un buon accordo in termini di risposta carico-spostamento, carico ultimo, quadro fessurativo e campi di deformazione.

Sia i modelli sezionali che quelli a tirante e puntone (S&T) sottostimano la capacità resistente, con questi ultimi che forniscono un'approssimazione migliore. Tuttavia, nessuno dei due approcci riesce a cogliere le differenze osservate nella campagna sperimentale tra le due configurazioni: la configurazione con due file di barre diagonali presenta una capacità resistente inferiore, nonostante abbia la stessa area totale di barre diagonali del caso con una sola fila. Anche il quadro fessurativo differisce tra le due configurazioni; tuttavia, questo confronto deve essere interpretato con cautela, poiché si basa su un singolo livello di carico, che per le due configurazioni corrisponde a due diversi stadi della risposta strutturale.

Ciò suggerisce che entrambi i modelli analitici presentano una sensibilità limitata all'influenza della distribuzione delle barre diagonali sui meccanismi interni di trasferimento del carico, evidenziando la necessità di ulteriori approfondimenti.

7 REFERENCES

Di Carlo, F., Meda, A., Molaioni, F. & Rinaldi, Z. 2023. Experimental evaluation of the corrosion influence on the structural response of Gerber half-joints. *Engineering Structures* (285): 116052.

Desnerck, P., Lees, J.M. & Morley, C.T. 2016. Impact of the reinforcement layout on the load capacity of reinforced concrete half-joints. *Engineering Structures* (127): 227–239.

DIANA FEA 2025. DIANA Finite Element Analysis User's Manual Release 10.10. *Delft, The Netherlands*.

fib – Fédération internationale du béton 2023. *fib Model Code for Concrete Structures 2020*. Ernst & Sohn, Lausanne, Switzerland.

Flores Ferreira, K., Rampini, M.C., Zani, G., Colombo, M. & di Prisco, M. 2023. Experimental investigation on the use of Fabric-Reinforced Cementitious Mortars for the retrofitting of reinforced concrete dapped-end beams. *Structural Concrete* (24)4.

Flores Ferreira, K., Rampini, M.C., Belletti, B., Calcavecchia, B., Camata, G., D'Angela, D., et al. 2025. Reinforced concrete dapped-end beams for existing bridges: Reliability of finite element models. *Structural Concrete* (26)4.

Gehri, N., Mata-Falcón, J. & Kaufmann, W. 2020. Automated crack detection and measurement based on digital image correlation. *Construction and Building Materials* (256): 119383.

Gehri, N., Mata-Falcón, J. & Kaufmann, W. 2022. Refined extraction of crack characteristics in large-scale concrete experiments based on digital image correlation. *Engineering Structures* (251): 113486.

Del Giudice, G. 1967. *Reinforced concrete bridge with dapped-end beams (in Italian).* Vitali e Ghianda (Ed). Genova.

Hendriks, M., de Boer, A. & Belletti, B. 2022. *Guidelines for Nonlinear Finite Element Analysis of Concrete Structures*. Rijkswaterstaat Centre for Infrastructure, Report RTD:1016-1:2022

Hordijk, D.A. 1991. Local approach to fatigue of concrete. Delft University of Technology

Mattock, A.H. & Chan, T.C. 1979. Design and behavior of dapped-end beams. *PCI journal* (24)6: 28–45.

Menichini, G., Gusella, F., Morano, S.G. & Orlando, M. 2025. RC dapped-end beams with various reinforcement layouts: An experimental investigation. *Engineering Structures* (322): 119043.

Menichini, G., Gusella, F. & Orlando, M. 2024. Methods for evaluating the ultimate capacity of existing RC half-joints. *Engineering Structures* (299): 117087.

di Prisco, M., Colombo, M. & Martinelli, P. 2023. Structural Aspects of the Collapse of a RC Half-Joint Bridge: Case of the Annone Overpass. *Journal of Bridge Engineering* (28)11: 5023007.

Santarsiero, G., Picciano, V. & Masi, A. 2023. Structural rehabilitation of half-joints in RC bridges: a state-of-the-art review. *Structure and Infrastructure Engineering*: 1–24.

Schlaich, J., Schäfer, K. & Jennewein, M. 1987. Toward a consistent design of structural concrete. *PCI journal* (32)3: 74–150.